Plasma dynamics in graphite and SWNT probed by inelastic electron and x-ray scattering

Christian Kramberger[*,1], Erik Einarsson[2], Simo Huotari[3], Therapool Thurakitseree[2], Shigeo Maruyama[2], Martin Knupfer[4] and Thomas Pichler[1]

[1] University of Vienna, Faculty of Physics, Strudlhofgasse 4, A-1090, Vienna, Austria
[2] University of Tokyo, Department of Mechanical Engineering, 7-3-1 Hongo, Bunkyo-ku, Tokyo 113-8656, Japan
[3] European Synchrotron Radiation Facility, Boîte Postale 220, F-38043 Grenoble Cedex 9, France
[4] IFW Dresden, Helmholtzstraße 20, D-01069 Dresden, Germany

Received 3 May 2010, revised XXXX, accepted XXXX
Published online XXXX

PACS 73.22.Lp

[*] Corresponding author: e-mail Christian.Kramberger-Kaplan@univie.ac.at, Phone: +43 1 4277 51369, Fax: +43 1 4277 51375

Graphite as well as bundled and freestanding single-walled carbon nanotubes (SWNTs) are allotropes of sp^2 carbon. However their dynamical structure factor $S(q,\omega)$ differs greatly because of the very different dimensionalities and geometries. Here $S(q,\omega)$ is experimentally accessed by means of inelastic x-ray and electron scattering. In our combined approach we utilize the equivalency and complementarity of the two techniques to access the dispersion relation of electronic inter-band transitions across the entire Brillouin zone. The extended range plasmon dispersions provide direct insight into the imprints of macroscopic screening and low-dimensional confinement on plasmons in SWNTs.

1 Introduction The graphene sheet is the basic building block of hierarchical materials such as graphite or single-walled carbon nanotubes (SWNTs). The latter are rolled-up strips of graphene and the former is a layered superstructure of individual flat graphene sheets. The versatile carbon sheets can be used to construct different macroscopic densities and even local dimensionalities. Either of these physical parameters, the local dimensionality as well as the macroscopic density are crucial for collective phenomena, such as charge-density waves [1, 2] or effective exciton binding energies [3,4]. Like any other quasi-particles quantized charge-density waves or plasmons can propagate in a solid, and posses a defined momentum state [5,6]. Experimentally they may be accessed by inelastic scattering probes. Formally all inelastic processes are described by the material specific loss-function that is for charged or electromagnetic probes readily derived from the complex dielectric function $\varepsilon(\omega)$ as $\phi(\omega) = \mathrm{Im}(-1/(\varepsilon(q,\omega)))$. The resonance frequency ω_p of a free electron gas occurs at $\omega_p^2 = n_e e^2/m_e\varepsilon_0$. The integral in the f-sum rule relates the total strength of the electronic response to ω_p by $\frac{\pi}{2}\omega_p^2 = \int d\omega\, \omega\phi(\omega)$. Noteworthy the overall strength scales with the macroscopic density of electrons n_e. Thus, plasmons are stiffened at increasing electron densities in the surrounding electronic medium. Due to this screening, a plasmon's energy $\hbar\omega$ always lies above the corresponding inter-band transition, or just at $\hbar\omega_p$ as in the case free electrons.

The electronic part of a material's loss-function is the sum of individual plasmon resonances. In conventional matter these resonances arise at the zeros of the real part of the generalized dielectric function $\mathrm{Re}(\varepsilon(q,\omega)) = 0$, that are upshifted with respect to electronic single particle transitions. In very dilute media, such as bare individual molecules and clusters or other isolated nano-objects, there is however an insufficient collective charge carrier density to cause real zeros in the general dielectric function $\mathrm{Re}(\varepsilon(q,\omega)) = 0$. In these cases the observed loss-peaks are no longer stemming from collective density waves in

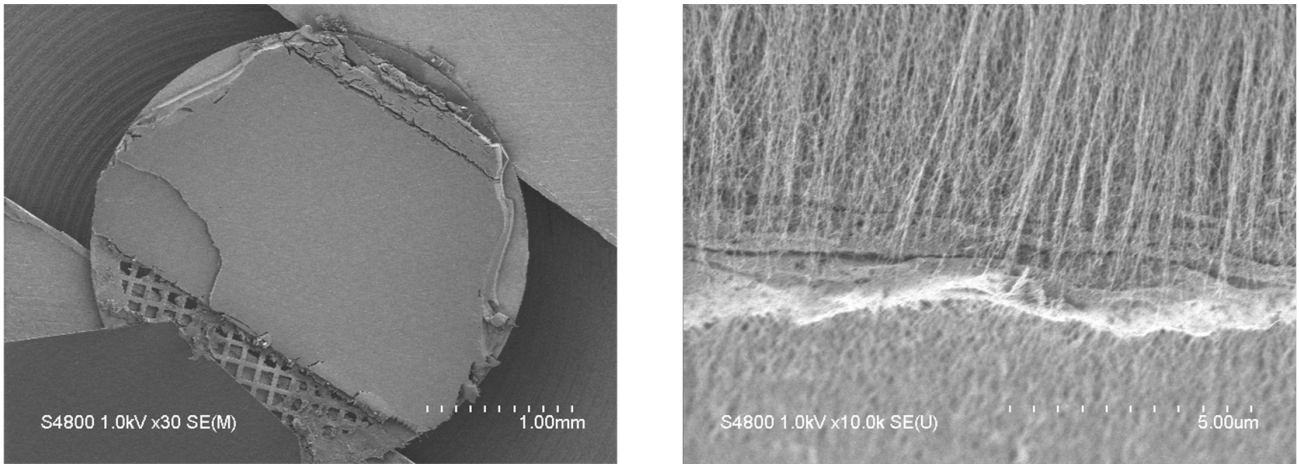

Figure 1 SEM micrographs of the double layered VA-SWNT film. The overview on the left hand side shows the large homogenous double layer. The close up on the interface of the two layers shows the aligned SWNT above and below. The micrographs were only taken after exposure to synchrotron radiation

a plasma but they are constituted of independent material-specific electronic inter-band transitions [7].

The momentum-dependent electronic loss function is commonly accessed by two entirely independent techniques. These two kinds of spectroscopies employ either inelastically scattered x-rays or electrons, both of which may excite propagating plasmons in the energy scale of eV and wavelengths in the range of $\mathring{A}$. Typical solids leave their fingerprints in these energetic and spatial ranges. Despite the deep fundamental analogy from the theory of inelastic scattering, both spectroscopies probe the loss-function in their own unique way. From an experimental point of view, especially regarding sample preparation and environmental control, the most crucial distinction lies in the magnitude as well as the different scaling of the cross-section with the scattering angle or momentum transfer q. The different magnitudes render electron energy loss spectroscopy (EELS) an ultra high vacuum method, while inelastic x-ray scattering (IXS) can be performed under ambient conditions. The utterly different scalings of the cross-sections are $\propto q^2$ for Thomson scattering and $\propto 1/q^2$ for Rutherford scattering of x-rays and electrons, respectively.

Here, we utilize archetypical sp^2 carbon systems like graphite and SWNTs to experimentally obtain the momentum resolved loss-function as probed in inelastic x-ray scattering (IXS). The results are compared to and discussed in respect to earlier studies of the momentum dependent loss-function as probed by angle-resolved electron energy-loss spectroscopy (AR-EELS) on graphite [8]. The methodical differences to other's earlier studies [9, 10, 11] are that we present the full angle resolved dispersion relation after combining IXS and AR-EELS. We find significantly modified plasmon dispersion in thin-bundled SWNTs [12] in comparison to bulk graphite. The lower absolute positions are connected to the diminutive dielectric screening and the change in the shape is an imprint of low-dimensionality. The very different shapes and also absolute energies are well displayed at small to intermediate momentum transfers q.

However in case of high q a uniform plasmon response is observed throughout any superstructure of sp^2 carbon sheets. We attribute these stark contrast between the low and the high q regimes to a wavelength dependent effective charge carrier density. The variant observed plasmon dispersions are imprints of the varied macroscopic electron densities in the internal morphologies as well as the local dimensionalities in the different superstructures of carbon sheets. Thus, nano-structured sp^2 carbon architectures are a showcase example of a widely tunable plasmon response and hence offer a significant potential for engineering optical properties.

2 Methods

2.1 Preparation Chemical vapor deposition (CVD) of static alcohol vapor on a shell structured Co/Mo catalyst [13] was used to grow $\sim$ 50 μm tall forests of vertically aligned SWNTs. As-grown films were floated off the quartz substrates by dipping the substrates into warm water and than re-captured on standard Cu TEM grids [14]. The catching of the film was performed twice to obtain a double layer. The total thickness of two vertically aligned SWNTs is $\sim$ 100 μm. The grid-supported SWNTs as well as empty TEM reference grids were mounted over a 2 mm wide slit in a 20x20x1 mm steel plate. A 500 μm thick sample of turbostratic graphite was used as a reference for archetypical bulk sp^2 carbon.

2.2 Loss-spectroscopy IXS experiments were conducted at beamline ID16 of the European Synchotron Radiation Facility (ESRF) in Grenoble[15]. The radiation from three undulators in a row was monochromatized by a liquid

nitrogen cooled Si(111) pre-monochromator and a Si(220) channel-cut secondary monochromator. Si(660) analyzer crystals were used in the Rowland-circle geometry with a bending radius of 1 m were used to disperse the inelastically scattered x-rays. The achieved energy resolution in the measurements was ∼0.75 eV. Depending on the orientation of the samples, spectra were either recorded in transmission or reflection geometry. In the former the momentum transfer is perpendicular to and in the latter q is parallel to the net alignment of the SWNTs. The momentum resolution was set by slitting the analyzers down to $\Delta q = 0.1\ \mathring{A}^{-1}$. The samples were measured at ambient temperature and under vacuum to reduce noise from spurious x-ray scattering on air.

2.3 Characterization The morphology of the vertically aligned SWNT (VA-SWNT) double layer was confirmed before and after IXS measurements by scanning electron microscopy (SEM, Hitachi S-4800 operated at 1 kV). Raman spectra of the as prepared double layers as well as the VA-SWNT after exposure to the high energy synchrotron irradiation were recorded at an excitation wavelength of 488 nm.

3 Results & Discussion

3.1 Morphology In Fig. 1 we show SEM micrographs of the double stacked VA-SWNT mats *after* IXS experiments were conducted. The images clearly show the morphology of a double layer of net-aligned SWNT. They evidence the morphology of the samples as thin bundles. Figure 2 compares the Raman spectra of the double layer samples before and after exposure the synchrotron irradiation. The pristine material shows the clear signature of SWNT with a broad diameter distribution in the RBM ranging from 100 up to 300 cm^{-1}, a small D line at 1342 cm^{-1} and a split G-line with G^- at 1567 cm^{-1} and G^+ at 1589 cm^{-1}. The G/D ratio of $\sim$ 25 is typical for as produced SWNT material. After x-ray irradiation the spectrum is completely changed. The RBM is gone and the broadened and approximately equally weak D and G line are observed upshifted at 1352 and 1593 cm^{-1}. This spectrum belongs to disordered sp^2. Note that there is no indication of sp^3 bonding environments in the spectra. From SEM and Raman we learn that our samples are net-aligned nano-wires of sp^2 carbon, the detailed internal structure of the thin bundles as individual parallel SWNT is not stable under irradiation, but they are transformed into templated nano-wires of all sp^2 carbon.

3.2 Loss-functions In Fig. 3 we compare the as measured IXS spectra of bulk turbostratic graphite and the VA-SWNT at various momentum transfers q. The nano-wires are measured in reflection geometry where q is along their net-alignment and the graphite is measured in transmission with q in the basal plane. The dispersive π plasmon is observed between energy losses of 7 and 12 eV, and the maximum of the $\pi + \sigma$ plasmon is observed in the range between 20 and 40 eV. The effective in-plane average of turbostratic graphite is in excellent agreement with earlier IXS studies on a graphitic single crystal [11].

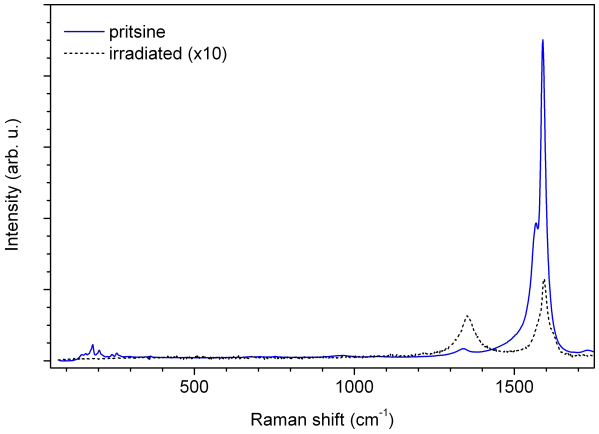

Figure 2 (color online) Raman spectra of the VA-SWNT films as measured at $\lambda = 488$ nm before (solid blue) and after (dashed black) exposure to synchrotron radiation

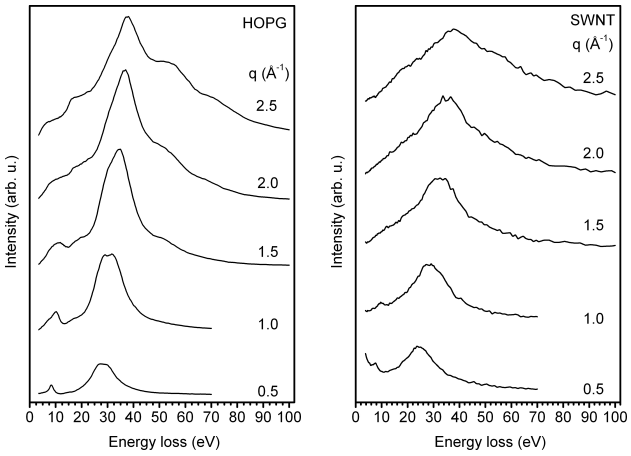

Figure 3 Loss-function as measured in IXS with $\hbar\omega = 9.688$ keV and different momentum tranfers q of highly ordered pyrolytic graphite (HOPG) on the left and single wall carbon na nanotubes (SWNT) on the right

3.3 Plasmon dispersions The dispersion of the $\pi + \sigma$ plasmon in either VA-SWNT or graphite is plotted in Fig. 4. The comparison of the $\pi + \sigma$ dispersion in graphite as measured in AR-EELS or IXS is also included. The $\sigma + \pi$ plasmon is clearly downshifted in the VA-SWNT as compared to the bulk material, because of the lower macroscopic density. Apparently this effect is not uniform across the entire dispersion relation. It is fully present at small q and fades out at high q, where the plasmon dispersions are no longer distinguishable. At these high q and accordingly short wavelengths $\lambda = 1/q$ the apparent local density inside the nano-wires equals that of bulk graphite.

The seamless joint of AR-EELS data, which is only available for small q, and IXS data for larger q demonstrates explicitly the equivalency and complementarity of the two methods. They are equivalent because they are both probing the same loss-function and they are complementary because of their different domains in q. The dispersion of the π plasmon is shown in Fig. 5. This time there is an discontinuity between the dispersion relation in turbostratic graphite (IXS) and a graphite single crystal (EELS). This is because the π electron system is not isotropic but rather trigonally warped in the plane. The shaded areas in Fig. 5 denote the realm of possible electronic interband transitions. We used tight binding parameters [16] that were fitted to GW-calculations and angle resolved photoemission experiments. The actual observation of a plasmon dispersion inside this dome underpins the importance of excitonic effects [3,4] in the electronic π systems of sp^2 carbon.

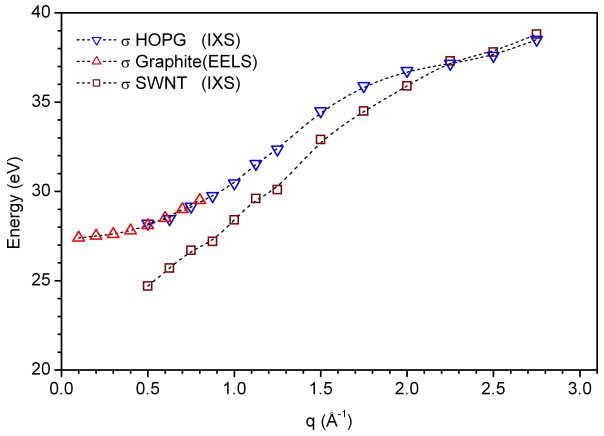

Figure 4 (color online) Dispersion of the $\pi + \sigma$ plasmon as measured in HOPG and VA-SWNT with IXS and a graphite single crystal as measured in angle resolved EELS

4 Summary We have explicitly demonstrated in the case of bulk graphite that inelastic electron and x-ray scattering are a quantitative match and that their powerful combination unlocks the observation of plasmon dispersions across the whole Brillouin zone. The comparison of bulk graphite with nano-wires of sp^2 carbon reveals wavelength dependent differences in their plasmon dispersions. The differences are well observed at long wavelengths that can actually probe the macroscopic density in a large volume, but at small wavelength the internal density of nano-wires is that of bulk sp^2. The varying screening is an imprint of the hierarchical inhomogeneities in the charge distribution.

Acknowledgements EE acknowledges support from the Global Center of Excellence for *Mechanical Systems Innovation* by the Japanese Ministry of Education, Culture, Sports, Science and Technology. TP acknowledges the DFG 440/3/5 and the FWF P21333-N20.

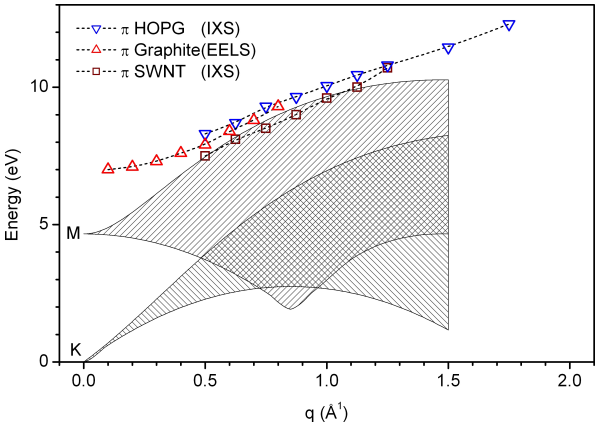

Figure 5 (color online) Dispersion of the π plasmon as measured in HOPG and VA-SWNT with IXS and a graphite single crystal as measured in angle resolved EELS

References

[1] S. DasSarma and E. H. Hwang, Phys. Rev. B **54**(3), 1936–1946 (1996).
[2] M. F. Lin, Phys. Rev. B **62**(19), 13153–13159 (2000).
[3] F. Wang, G. Dukovic, L. E. Brus, and T. F. Heinz, Science **308**(5723), 838–841 (2005).
[4] C. D. Spataru, S. Ismail-Beigi, R. B. Capaz, and S. G. Louie, Quasiparticle and excitonic effects in the optical response
of nanotubes and nanoribbons, Topics in Applied Physics, Vol. 111 (Springer Verlag, Berlin Heidelberg, 2008).
[5] P. Nozieres and D. Pines, Phys. Rev. **113**(5), 1254 (1959).
[6] G. Onida, L. Reining, and A. Rubio, Rev. Mod. Phys. **74**, 601 (2002).
[7] H. Raether, Excitation of Plasmons and Interband Transitions by Electrons, Springer Tracts Mod. Phys., Vol. 88 (Springer Verlag, Berlin Heidelberg, 1980).
[8] A. G. Marinopoulos, L. Reining, V. Olevano, A. Rubio, T. Pichler, X. Liu, M. Knupfer, and J. Fink, Phys. Rev. Lett. **89**(7), 076402 (2002).
[9] M. Kociak, L. Henrard, O. Stephan, K. Suenaga, and C. Colliex, Phys. Rev. B **61**(20), 13936–13944 (2000).
[10] M. H. Upton, R. F. Klie, J. P. Hill, T. Gog, D. Casa, W. Ku, Y. Zhu, M. Y. Sfeir, J. Misewich, G. Eres, and D. Lowndes, Carbon **47**(1), 162–168 (2009).
[11] N. Hiraoka, H. Ishii, I. Jarrige, and Y. Q. Cai, Phys. Rev. B **72**(7), 075103 (2005).
[12] E. Einarsson, H. Shiozawa, C. Kramberger, M. H. Rummeli, A. Gruneis, T. Pichler, and S. Maruyama, J. Phys. Chem. C **111**(48), 17861–17864 (2007).
[13] H. Oshima, Y. Suzuki, T. Shimazu, and S. Maruyama, Jap. Jour. Appl. Phys. **47**(4), 1982–1984 (2008).
[14] Y. Murakami and S. Maruyama, Chem. Phys. Lett. **422**(4-6), 575–580 (2006).
[15] R. Verbeni, T. Pylkkänen, S. Huotari, L. Simonelli, G. Vankó, K. Martel, C. Henriquet, and G. Monaco, J. Synchotron **16**(4), 469–476 (2009).
[16] A. Gruneis, C. Attaccalite, L. Wirtz, H. Shiozawa, R. Saito, T. Pichler, and A. Rubio, Phys. Rev. B **78**(20), 205425 (2008).